Cell PRESS
Neuron
Article

Robust Odor Coding via Inhalation-Coupled Transient Activity in the Mammalian Olfactory Bulb

Kevin M. Cury[1] and Naoshige Uchida[1,*]
[1]Center for Brain Science, Department of Molecular and Cellular Biology, Harvard University, 16 Divinity Avenue, Cambridge, MA 02138, USA
*Correspondence: uchida@mcb.harvard.edu
DOI 10.1016/j.neuron.2010.09.040

SUMMARY

It has been proposed that a single sniff generates a "snapshot" of the olfactory world. However, odor coding on this timescale is poorly understood, and it is not known whether coding is invariant to changes in respiration frequency. We investigated this by recording spike trains from the olfactory bulb in awake, behaving rats. During rapid sniffing, odor inhalation triggered rapid and reliable cell- and odor-specific temporal spike patterns. These fine temporal responses conveyed substantial odor information within the first ~100 ms, and correlated with behavioral discrimination time on a trial-by-trial basis. Surprisingly, the initial transient portions of responses were highly conserved between rapid sniffing and slow breathing. Firing rates over the entire respiration cycle carried less odor information, did not correlate with behavior, and were poorly conserved across respiration frequency. These results suggest that inhalation-coupled transient activity forms a robust neural code that is invariant to changes in respiration behavior.

INTRODUCTION

Sensation is constructed through dynamic sampling of the external world, as exemplified by the saccadic eye movements that underlie visual perception, or active touch in somatosensation. In olfaction, sensory input is dynamically regulated by respiration behavior. Animals exhibit a rich repertoire of olfactory sampling behavior depending on behavioral context (Kepecs et al., 2007; Welker, 1964; Youngentob et al., 1987). During exploration, many animals partake in stereotyped and rhythmic high-frequency respiration in the theta frequency range ("rapid sniffing," 6–10 Hz in rats), distinct from the slow breathing that is generally observed during rest (1–2 Hz). Psychophysical experiments have demonstrated that a single rapid sniff (~160 ms) can support accurate olfactory discrimination, positing that the neural activity within a single sniff cycle provides a relatively complete perceptual "snapshot" (Karpov, 1980; Kepecs et al., 2006; Rajan et al., 2006; Uchida and Mainen, 2003; Wesson et al., 2008a). However, very little is known about the nature of neural activity during natural sampling behavior (Rinberg and Gelperin, 2006; Verhagen et al., 2007; Wilson and Mainen, 2006), leaving unanswered questions as to (1) how odors are encoded on the timescale of a single sniff, and (2) what role sampling dynamics play in terms of neural coding.

The olfactory bulb (OB) is an attractive target for addressing these questions, as it is the exclusive recipient of input from olfactory receptor neurons in the nose. Furthermore, the output of the OB—transmitted by mitral and tufted (M/T) cells—is directly broadcast to numerous higher brain centers (e.g., piriform cortex, amygdala, and entorhinal cortex). As such, the spike trains of M/T cells represent the neural code that communicates everything the rest of the brain needs to know about the olfactory environment. It has been observed that M/T cells respond with cell- and odor-specific patterns of spikes whose temporal structure fluctuates on timescales faster than the stimulus itself (e.g., in response to a constant odor pulse) (Friedrich and Laurent, 2001; Friedrich and Stopfer, 2001; Hamilton and Kauer, 1989; Mazor and Laurent, 2005; Meredith and Moulton, 1978; Wehr and Laurent, 1996). This has led to the view that such patterned sequences of activity may constitute a "temporal code" for conveying information about odor identity to downstream brain centers. However, this idea has primarily been developed in anesthetized rodents, as well as insect and fish preparations, and it is debated whether the brain actually makes use of these patterns for guiding behavior. Furthermore, it is not known whether such a coding scheme is applicable in the face of active sampling behaviors, such as respiration, that introduce variable and complex dynamics to the stimulus (Mainen, 2006; Uchida and Mainen, 2003; Wilson, 2008).

Regarding the impact of respiration behavior, it has long been observed that both spontaneous activity and odor-induced activity of M/T cells are temporally modulated by the breathing rhythm (Cang and Isaacson, 2003; Chaput, 1986; Fantana et al., 2008; Macrides and Chorover, 1972; Margrie and Schaefer, 2003; Meredith, 1986; Spors and Grinvald, 2002; Wellis et al., 1989). However, a recent study has posed a serious challenge to the relevance of these respiration-coupled patterns for odor coding (Bathellier et al., 2008). Based on the responses of a population of M/T cells, they concluded that the majority of odor information can be extracted from the mean firing rate over the respiration cycle, and that accounting for finer-scale temporal features added little additional information (Bathellier et al., 2008). It is important to note, however, that this and the vast majority of previous experiments were done using anesthetized animals, where respiration sampling is low in frequency and stereotyped.

While there is some evidence that, under more dynamic stimulus conditions, neurons in the locust antennae lobe (an OB analog) exhibit reliable temporal responses (Brown et al.,

2005), studies in awake mammals have argued that neural activity in the OB is largely decoupled from the respiration rhythm during active modes of sampling behavior (i.e., rapid sniffing) (Bhalla and Bower, 1997; Carey et al., 2009; Kay and Laurent, 1999; Verhagen et al., 2007). This body of work has led to the view that subsniff spike timing may not be relevant for odor coding during rapid sniffing, and that unique coding strategies may exist between rapid sniffing and slow breathing. In part, these viewpoints are based on neural recordings made under less controlled stimulus presentations or over multiple respiration cycles. However, given the speed with which animals can identify and react to odors (Karpov, 1980; Kepecs et al., 2007; Rajan et al., 2006; Uchida and Mainen, 2003; Wesson et al., 2008a), the sensory response to the first encounter with an odorant appears crucial and sufficient for guiding many behavioral decisions. To our knowledge, no study to date has evaluated the impact that natural respiration dynamics have on M/T cell odor coding during this key first encounter with an odorant. Furthermore, these matters have not been addressed in the context of the decision process, which can provide critical insight into the salient features of neural responses (Britten et al., 1996; Luna et al., 2005; Parker and Newsome, 1998).

Here we recorded spike trains from individual M/T cells simultaneously with the ongoing respiration rhythm of awake, behaving rats while they performed two distinct modes of odor sampling: rapid sniffing and slow breathing (Experimental Procedures; Figure S1 available online). Rapid sniffing responses were recorded while the animals performed an odor discrimination task, and here we found that the first inhalation of an odorant evoked reliable and cell-specific spike patterns within the time course of a single rapid sniff. These subsniff patterned responses conveyed significantly more odor information in their fine-scale fluctuations (20–40 ms timescale) as compared with their total spike count, and correlated with behavioral reaction time on a trial-by-trial basis. Furthermore, we identified that the initial portions of these patterns were highly conserved between rapid sniffing and slow breathing odor responses.

RESULTS

Data were collected as rats performed either of two behavioral paradigms meant to emphasize distinct modes of odor sampling—rapid sniffing and slow breathing. The rapid-sniffing paradigm entailed a two-alternative choice odor discrimination task (Movie S1 available online) (Uchida and Mainen, 2003), and in the slow-breathing paradigm, odors were presented to the animals while they maintained their snout in an odor port (Movie S2). We begin our report with a description of results from the discrimination task.

M/T Cells Respond to Odors with Fine Temporal Spike Patterns during Rapid Sniffing

We recorded a total of 232 well-isolated M/T cells in five rats while performing a discrimination task, where it has been demonstrated that animals reliably exhibit rapid sniffing during odor sampling (Kepecs et al., 2007; Uchida and Mainen, 2003; Wesson et al., 2008b). On a given trial, the animal must sample an odor stimulus and then choose the water port that is associated with the stimulus for water reward (Figures 1A and 1B, see Experimental Procedures). The animals discriminated among a fixed panel of six odors. Additionally, in some trials, a pure air, "blank" stimulus was used for control measurements. We sought to determine whether single neurons responded with odor-specific patterning within the timescale of a single sniff. We first generated perievent time histograms (PETHs) of single-cell responses aligned to the onset of the first odor inhalation using either a narrow (10 ms) or broad (100 ms) temporal filter (Figure 1C). While high-frequency features of the odor response diverged from those of the blank control, slower features appeared largely unchanged. This observation suggests that approaches that (1) measure response over slower timescales, or (2) fail to account for the timing imposed by the respiration rhythm will blur out features of the neural response.

Next, we more carefully considered the activity occurring over the first 160 ms following odor inhalation onset—a window of time that approximates a single rapid sniff (1/160 ms = 6.25 Hz; Figures 1D and 1E). While some responses exhibited a clear increase in total spike count (see Figures 1D and 1E, odor D), other responses appeared simply as a temporal redistribution of spikes in comparison to the pure-air stimulus (see Figures 1D and 1E, odor A). To quantify this, we identified odor responses that produced significant changes from the blank control using the following two methods: a "rate" response was defined as a significant increase or decrease in total spike count over the entire 160 ms window ($p < 0.05$, Wilcoxon rank sum test), and a "temporal" response was identified when the distribution of spike times within the 160 ms window differed significantly from that of the blank control ($p < 0.05$, Kolmogorov-Smirnov test).

Across the population, 15% of neuron-odor pairs exhibited rate responses, while 13% were shown to be temporally modulated (Figure 1F). Interestingly, a large fraction (62%) of temporal responses occurred in the absence of a significant change in rate. These responses were distributed across the stimulus panel (Figure 1G), with 50% of neurons exhibiting at least one temporal response, and 69% responding to at least one odor by either metric (Figure 1H). In total, these results demonstrate that during the first sniff of an odor, a large proportion of M/T cells respond with fine temporal spike patterns that are coupled to inhalation onset, and occur in part without an impact on their total spike count.

Temporal Response Patterns Are Reliable and Diverse across Neurons and Odors

We sought to further characterize the diversity of temporal responses, both across odors for individual neurons, and across neurons for a given odor. Figure 2A illustrates the activity of five M/T cells in response to three odors and the blank control. Individual responses consist of transient epochs of increased and/or decreased instantaneous firing rate. Furthermore, a given neuron is capable of responding to multiple odors with unique patterns of activation. Neurons can exhibit excitation in response to multiple odors, but with unique timing and magnitude (e.g., neurons 1 and 4 in Figure 2A). Additionally, they can be inhibited by odor stimulation, in some cases responding with some combination of both excitation and inhibition to different odors

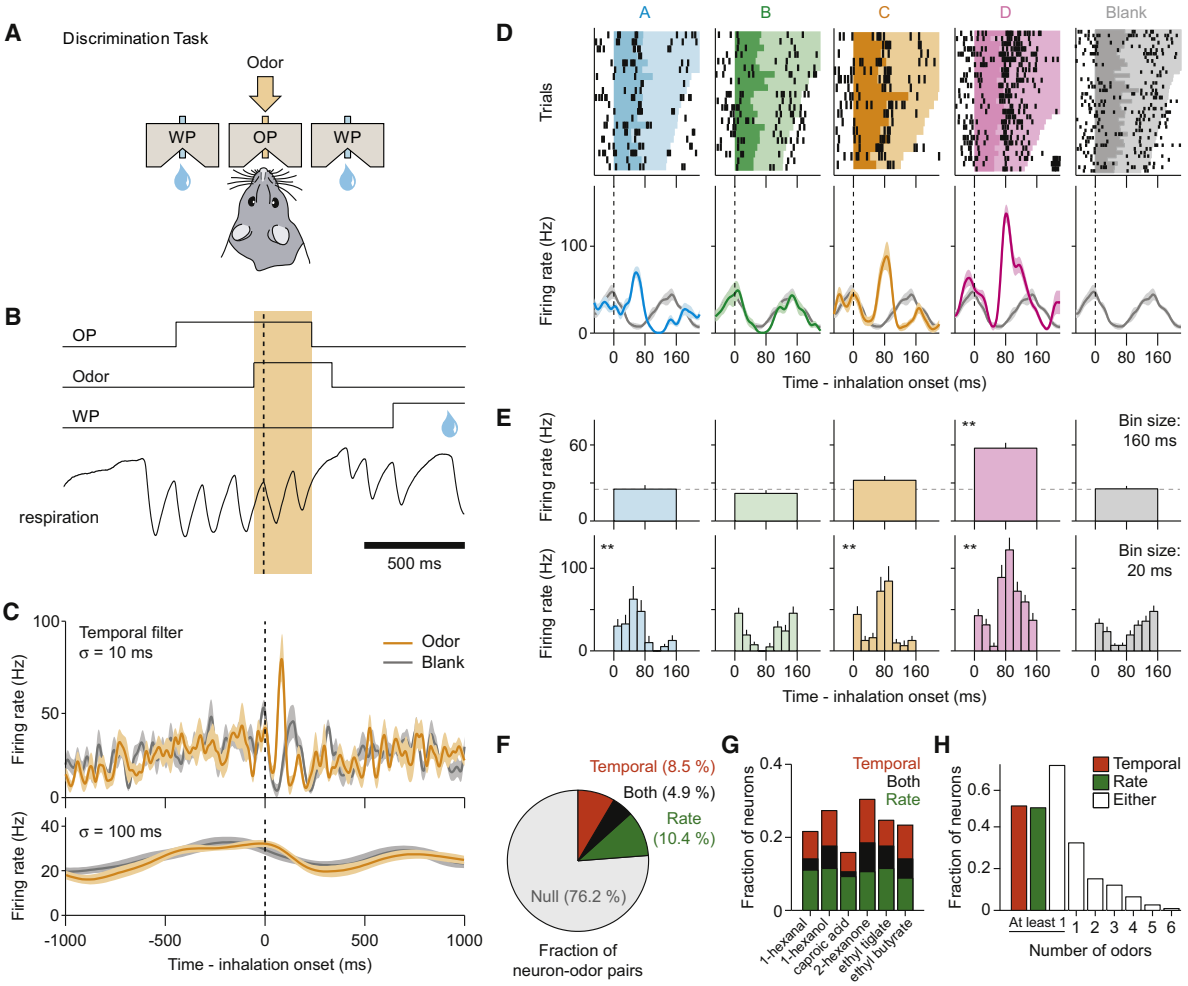

Figure 1. M/T Cells Respond to Odors with Subsniff Spike Patterns Locked to Inhalation Onset

(A) Two-alternative choice odor discrimination task. Central odor port (OP) and water reward port (WP) are shown.

(B) Task diagram (top) and respiration behavior (bottom). Downward and upward deflections of the respiration trace reflect inhalation and exhalation, respectively. Orange shading, odor presentation.

(C) Perievent time histogram (PETH) of an example M/T cell, aligned by the onset of the first inhalation after odor valve opening. Orange, butyraldehyde; gray, "blank" control. The firing rates were smoothed using a Gaussian filter (top: SD = 10 ms; bottom: SD = 100 ms). The mean ± SE are plotted for this and all subsequent PETHs.

(D) Spike patterning of the same M/T cell. Top: raster plots of spike trains. Each row corresponds to a single trial, with vertical tick marks indicating the occurrence of a spike. Trials are aligned by the first odor inhalation onset, and are sorted from bottom to top in terms of increasing respiration duration. In this and subsequent raster plots, the colored shading indicates the first respiration cycle after odor onset, with the darker shading corresponding to the inhalation period. Bottom: corresponding PETHs calculated using a Gaussian filter (SD = 7.5 ms; utilized for all subsequent PETHs unless otherwise noted). Odors: A, 1-hexanal; B, ethyl tiglate; C, butyraldehyde; D, R(-)-2-octanol. The blank PETH (gray) is plotted in all panels.

(E) For the same M/T cell and odors, PETHs were generated over the 0–160 ms window following odor inhalation onset at two different temporal resolutions. Top: total spike count over a single 160 ms bin. The horizontal dashed line denotes the mean spike count of the blank control. Bottom: eight nonoverlapping 20 ms bins. Asterisks in the top and bottom graphs indicate rate and temporal responses, respectively.

(F) Fraction of neuron-odor pairs that showed temporal (orange; $p < 0.05$, Kolmogorov-Smirnov test) or rate responses (green; $p < 0.05$, Wilcoxon rank sum test), with the overlap indicated in black ("both"). The "null" fraction (gray) did not elicit a significant response. Data are from 1392 neuron-odor pairs (232 neurons, six odors).

(G) Per-stimulus fraction of neurons that showed temporal, rate, or both response types.

(H) Fraction of neurons that responded to at least one odor with a temporal response, with a rate response, or by either measure. Additionally plotted is the fraction that responded by either measure to a specific number of odors in the panel.

(e.g., neuron 2). Considering the response of multiple M/T cells to a single odor, we observe diversity in both the timing and magnitude of spiking activity. All together, these observations suggest that collective subpopulations of M/T cells represent different odors with unique spatio-temporal activity patterns that fluctuate rapidly within a single rapid sniff cycle (Figure 2B).

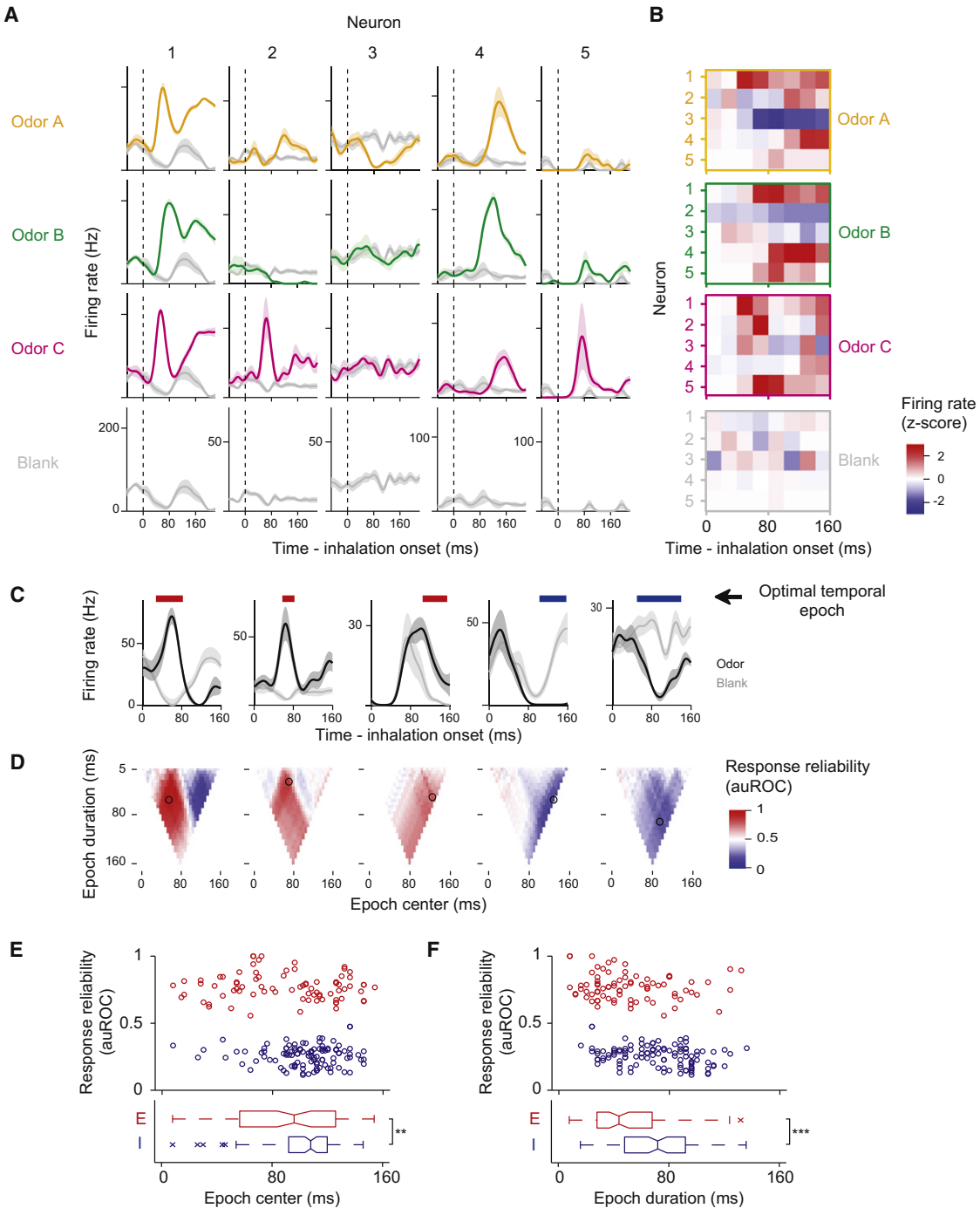

Figure 2. Odor-Evoked Temporal Responses Are Diverse and Reliable

(A) PETHs of five example M/T cells (mean ± SE). Odors: A, 2-hexanone; B, ethyl butyrate; C, ethyl tiglate. Gray: blank.

(B) Population PETHs. Each panel shows PETHs of the same five M/T cells to one of the four stimuli. PETHs were generated using eight nonoverlapping 20 ms bins. Firing rates are normalized using z-scores, with 0 indicating the mean firing rate of the blank control.

(C) The optimal temporal epoch for five example neuron-odor pairs. Red, excitatory; blue, inhibitory. Black PETH, odor; gray PETH, blank.

(D) Response reliability (area under the ROC curve, or auROC) calculated for varying temporal epochs (bin size: 5 ms to 160 ms; bin center: t = 0 to t = 160 ms). Red and blue signify increased and decreased spike counts, respectively. Black circle: the optimal temporal epoch. Epochs were selected not to exceed the bounds of 0 to 160 ms following odor inhalation onset.

(E) Distribution of the center of the optimal temporal epoch plotted against response reliability for all significant temporal responses (n = 186 neuron-odor pairs). Red, excitatory; blue, inhibitory. The bottom graph shows box plots for excitatory (E) and inhibitory (I) responses. **p < 0.01, t test.

(F) Distribution of the duration of the optimal temporal epoch plotted against response reliability. ***p < 0.0001.

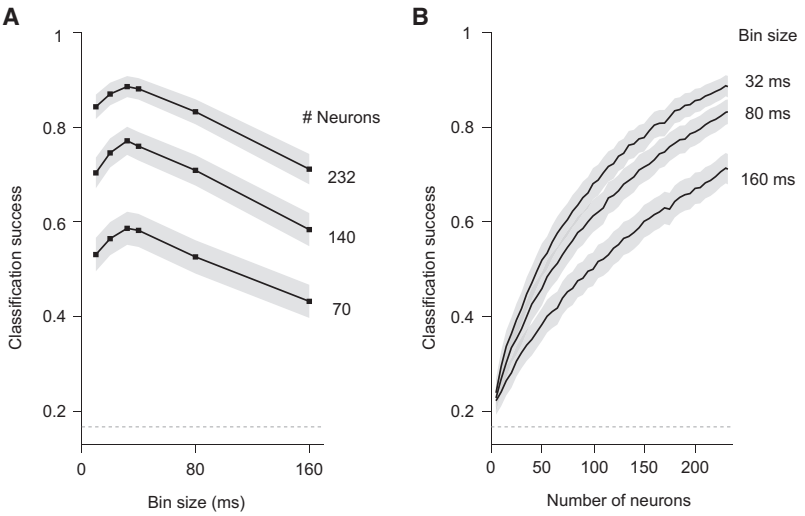

Figure 3. Accounting for Subsniff Response Patterns Improves the Discrimination Performance of a Linear Classifier

(A) Performance of a linear classifier in discriminating between six odors based on population neural activity over the 160 ms window following the first odor inhalation, plotted as a function of bin size (10 ms to 160 ms, i.e., temporal resolution). The results for three different population sizes are plotted separately. In this and the next panel, the black trace and gray shading represent the mean ± SE over repeated permutations of cell and trial combinations. The dashed gray line indicates chance performance (1/6 = 16.7%).

(B) The same results as (A), plotted as a function of the number of neurons.

Next we sought to determine the reliability of these response patterns across trials. Specifically, we quantified how well we could discriminate between single-trial spike-count distributions of odor responses from the blank control using the receiver-operating characteristic (ROC) analysis, a method based on signal detection theory. This analysis quantifies the overlap between two distributions in terms of the accuracy with which an ideal observer can discriminate between single presentations of the two conditions (Green and Swets, 1966). The overlap between spike-count distributions was compared over a range of temporal epochs within the first sniff cycle (bins ranging from 5 to 160 ms scanned over the 160 ms response window, in 2 ms steps; Figures 2C, 2D, and S2). Using this metric, perfect discrimination results in a value of 1 or 0 (for increases or decreases in spike count, respectively) with 0.5 indicating completely overlapping distributions. For each neuron-odor pair, we identified the optimal temporal epoch that produced maximal discrimination, and classified the response as excitatory or inhibitory depending on its sign within this epoch (Figures 2E and 2F). Interestingly, excitatory epochs were more short-lived and distributed throughout the respiration cycle, whereas inhibitory epochs typically occurred with more delayed timing and were of longer duration (epoch center, $p < 0.01$, epoch duration, $p < 0.0001$, t test). In summary, M/T cells respond to odors reliably and with broad diversity in terms of the sign, magnitude, and timing of spiking activity.

Subsniff Temporal Patterns Convey Substantial Odor Information

As M/T cells are the exclusive output neurons of the OB, downstream brain centers must discriminate between odors based solely on the spiking activity of M/T cells. Furthermore, the brain must perform these discriminations based on single stimulus presentations, integrating the spike trains of large populations of neurons in real time. Here, we sought to determine the impact of subsniff activity patterns, described above, from the perspective of a downstream odor classifier. Using a linear classification method, we quantified how accurately single-trial responses from a population of neurons could be used to discriminate the identity of an odor. We considered only the first 160 ms after odor inhalation, and explored the impact of subsniff activity at different resolutions by varying the window size used to bin spike trains.

To evaluate the discriminability of responses on slow timescales, we generated activity vectors composed of single-trial total spike counts over the entire 160 ms window for all 232 neurons. Finer temporal features were accounted for by dividing this window into smaller bins. One trial from each odor response was withheld and the remainder were used to train the classifier (see Experimental Procedures). Utilizing total spike count (160 ms bin size), the classifier achieved moderate success, identifying the stimulus correctly 71% of the time (Figures 3A and 3B; for controls, see Figure S3). In contrast, by subdividing the window into five 32 ms bins, we observed a marked improvement, achieving 89% success. Thus, these results demonstrate that subsniff spike patterns of M/T cells are most informative about the identity of an odor when read out at a resolution of 20–40 ms.

M/T Cell Population Exhibits Rapid Response Dynamics within a Single Sniff

To gain insight into the dynamics of this population response, we visualized average population activity using principal component analysis, a dimensionality reduction method. Figure 4A shows trajectories of the mean response of the 232 neuron population to three odors and the blank control, represented as projections onto the first three principal components. After ~30 ms following inhalation onset, odor response trajectories rapidly diverge from baseline and from one another (30–60 ms). Subsequent to this, the responses evolved, not simply returning to baseline but rather tracing out paths that are unique from the initial excursion (60–160 ms).

To quantify these observations, we first measured the instantaneous separation between population odor responses

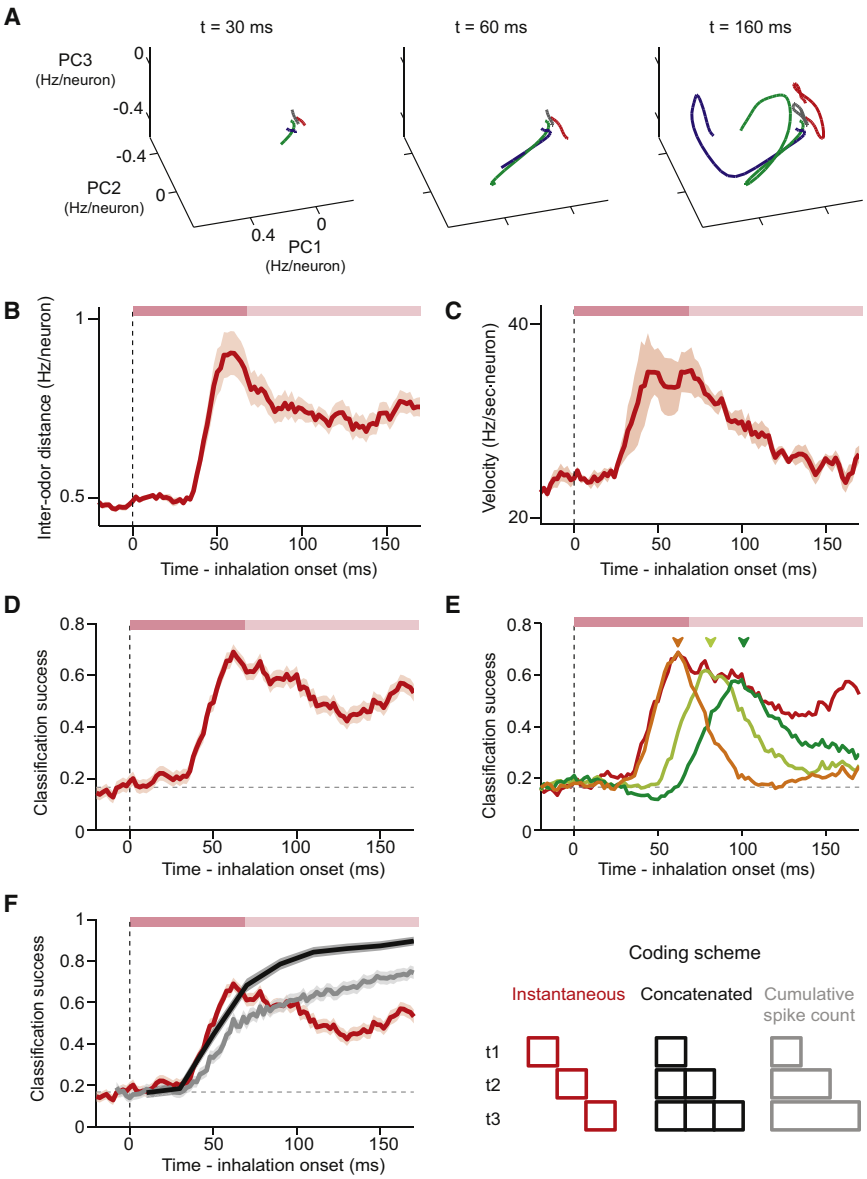

Figure 4. Odor Information Is Distributed over the Time Course of Rapidly Evolving M/T Cell Population Response

(A) Visualization of M/T cell population responses using principal component analysis (n = 232 M/T cells). The responses to three odors are projected onto the first three principal components. Odors: red, 1-hexanal; green, ethyl tiglate; blue, ethyl butyrate. Gray: blank.

(B) Distance between M/T cell population responses (15 pairwise combinations of the six odors, mean ± SE). In this and subsequent panels, the median inhalation duration (68 ms) and median respiration duration (172 ms) of the first sniff are indicated by the dark and light red shaded bars, respectively, shown at top.

(C) Rate of change (velocity) of M/T cell population responses (six odors, mean ± SE).

(D) Time course of the performance of a linear classifier based on instantaneous activity patterns (20 ms sliding window, mean ± SE).

(E) Classification accuracy is highly sensitive to temporal shifts. A linear classifier was trained at a given time point (orange, 62 ms; light green, 82 ms; dark green, 102 ms; see arrowheads), and its performance was evaluated with temporally offset test data. The red trace is as in (D).

(F) Comparison of the performance of a linear classifier across three different coding schemes (mean ± SE), depicted in schematic at right. Red, "Instantaneous" bins, as in (D); gray, "Cumulative spike count," testing and training data consisting of spike counts over the window from 0 to t; black, "Concatenated" bins, testing and training data consisting of incrementally concatenated 20 ms nonoverlapping bins from 0 to t.

(Figure 4B; Mazor and Laurent, 2005; Stopfer et al., 2003). The separation reached a maximum at ~60 ms, and subsequent to this peak, the distance between odors diminished, while remaining above baseline levels throughout the rest of the respiration cycle. We additionally calculated the rate at which population activity vectors changed over subsequent time steps (20 ms time bins; Figure 4C) (Mazor and Laurent, 2005). This rate rapidly increased to a maximum within ~45 ms. This state of high velocity persisted through ~80 ms post inhalation onset before gradually returning to baseline levels near the end of the respiration cycle. Therefore, throughout the period during which odors are separable, the responses continued to evolve, reflecting the temporally staggered excitatory and inhibitory epochs observed at the single-cell level (Figures 2E and 2F).

Odor Information Is Distributed over the Time Course of a Sniff

The ability of a downstream brain center to discriminate between odors based on these fine-scale patterns additionally depends on the trial-to-trial reliability of responses at different points along this evolution. To address this we used a linear classifier as above (Figure 3), but instead we binned the spike trains over a short sliding window (20 ms). Consistent with the time course of inter-odor distance (Figure 4B), classification success rate rapidly rises and reaches a maximum at ~60 ms (Figure 4D). Afterwards, performance is degraded, but remains relatively high for the remainder of the sniff cycle, resulting in a more uniform profile than we expected, considering the sharp peak observed in Figure 4B.

Based on the observation that population responses continually evolve over the course of a single sniff (Figures 4A and 4C), we additionally expected that independent odor information would be available at different time points within the sniff cycle. One predictor of this is that a classifier derived from a given instant will poorly generalize across time. To quantify this, we examined how the success rate of a classifier degraded when

testing was performed with activity vectors taken from time points further and further away. This demonstrated that a classifier derived near the peak discrimination accuracy was the most sensitive to temporal shifts, degrading to half-maximum performance within just 30 ms (Figure 4E, orange, and Figures S4A and S4B). Thus, fine-scale odor representations evolve as a sequence of informative patterns that become dissimilar from themselves over the course of a single sniff.

If different time points do indeed contain independent information, combining activity from subsequent stages of the response should further improve discrimination accuracy. To test this, we performed a similar analysis to that in Figure 4D; however, instead of considering each time point in isolation, we concatenated adjacent nonoverlapping bins (see schematic at right in Figure 4F, black). With this approach, the success rate was closely matched to that of isolated bins up to the peak that was observed near 60 ms. However, as additional bins were added subsequent to this point, classification performance continued to improve, quickly increasing to 82% after 100 ms (five 20 ms concatenated bins). For contrast, we also considered a classifier based on cumulative spike counts (Figure 4F, gray). Relative to the concatenated approach, we achieved poor discrimination using this method despite the fact that the same number of spikes was used in both cases. In total, these results suggest that the improvement in odor discrimination achieved by considering fine-scale temporal features within a sniff cycle (Figure 3) can be attributed to the observation that different timepoints along the rapidly evolving population response contain nonredundant information.

Subsniff Response Patterns Correlate with Behavioral Reaction Time

The question remains as to whether these fine-scale temporal features actually contribute to behavioral odor discriminations. This question can be addressed by considering correlations between neural activity and behavior (Britten et al., 1996; Luna et al., 2005; Parker and Newsome, 1998). In our discrimination task, the animal is free to make its choice at any point following odor onset (Figure 1A). Thus, after first encounter with the stimulus, the animal must decide whether to exit from the odor sampling port and commit to a choice, or to take another sniff. The animals exhibited variable reaction times across odor trials, sampling the stimulus with 1.90 ± 0.10 sniffs (mean ± SD), where 32.8% ± 6.0% of trials consisted of just one sniff (mean ± SD, n = 4 rats; Figure 5A). Given that task performance for single-sniff trials does not differ significantly from that of multiple-sniff trials (Figure 5B) (Uchida and Mainen, 2003), it is possible that the animals obtained more stimulus information during the first sniff cycle when they made a choice after just one sniff. Here we test this prediction, which is consistent with various models of perceptual decision making that posit that a decision is postponed until the animal has gained sufficient sensory evidence (Gold and Shadlen, 2007; Luce, 1986; Smith and Ratcliff, 2004; Watson, 1979).

Figure 5C illustrates the responses of an M/T cell to an odor for both single- and multiple-sniff trials. This cell responded more vigorously for single-sniff trials. To examine whether this was the case across the pool of temporal responses (Figure 1F), we compared average response magnitudes over the optimal temporal epoch. This epoch was identified for each neuron-odor pair as described above (see Figures 2C and 2D), though it was restricted to occur within a shorter window (from 0 to 120 ms after inhalation onset). Because the median onset time of the second sniff in multiple-sniff trials was 153 ± 14 ms (mean ± SD, n = 4 rats; Figure S5I), we chose to restrict our analysis to a window of time that could influence the animal's decision to take another sniff. The response magnitude was calculated as the average change in spike count from the blank control within the identified epoch. Single-sniff responses were significantly larger in magnitude for both excitatory and inhibitory epochs (Figures 5D and 5E; $p < 0.01$ for both groups, one-tailed paired t test; for inhibitory epochs, we defined a larger response magnitude as a decreased spike count). When we performed the same analysis using total spike counts over the entire 120 ms window for the pool of rate responses, we did not observe a significant difference in response magnitude between single- and multiple-sniff trials (Figures S5A and S5B; $p > 0.2$ for both excitation and inhibition, one-tailed paired t test). Thus, responses over subsniff epochs, and not over prolonged windows, appear to correlate with behavioral reaction time.

We next determined the reliability of this relationship by examining single-trial responses of individual M/T cells. To quantify this, we used the ROC analysis to test the ability to distinguish between responses of individual single- and multiple-sniff trails. This approach is analogous to the so-called "choice probability" analysis commonly used to measure neural and behavioral correlations in the visual system (e.g., Britten et al., 1996). The area under the ROC curve was calculated over distributions of single-trial spike counts within the same window conditions as above. Applied in this manner, a value of 1 indicates that response magnitudes were larger in every trial of single-sniff trials, with 0.5 indicating perfectly overlapping distributions (for inhibitory responses, as above, we defined an increased response magnitude as a reduction in spike count). We asked whether the mean of these values across the pool of responses was significantly more positive than 0.5. We found this to be the case for temporal responses (Figures 5F and 5G; $p < 0.01$ for both excitatory and inhibitory epochs, t test), but not for rate responses (Figures S5C and S5D; $p > 0.6$ and $p > 0.1$ for excitation and inhibition, respectively, t test). Thus, temporal responses correlate with behavioral reaction time on a trial-by-trial basis, and interestingly, the degree of this correlation is comparable to what has been reported for choice probabilities in the visual system (e.g., Britten et al., 1996; Cohen and Newsome, 2009).

These observations should mean that first-sniff odor responses are more discriminable for single-sniff trials as compared with those of multiple-sniff trials, but only when considering fine-scale activity patterns. To test this, we performed a linear classification analysis using the same three coding schemes as before (see Figure 4F), though now we separately computed success rates for single-sniff and multiple-sniff test trials (Figure 5H). Classification accuracy was significantly higher for responses from single-sniff trials as compared with that of responses from multiple-sniff trials for the two coding schemes that take into account fine-scale activity, but not for

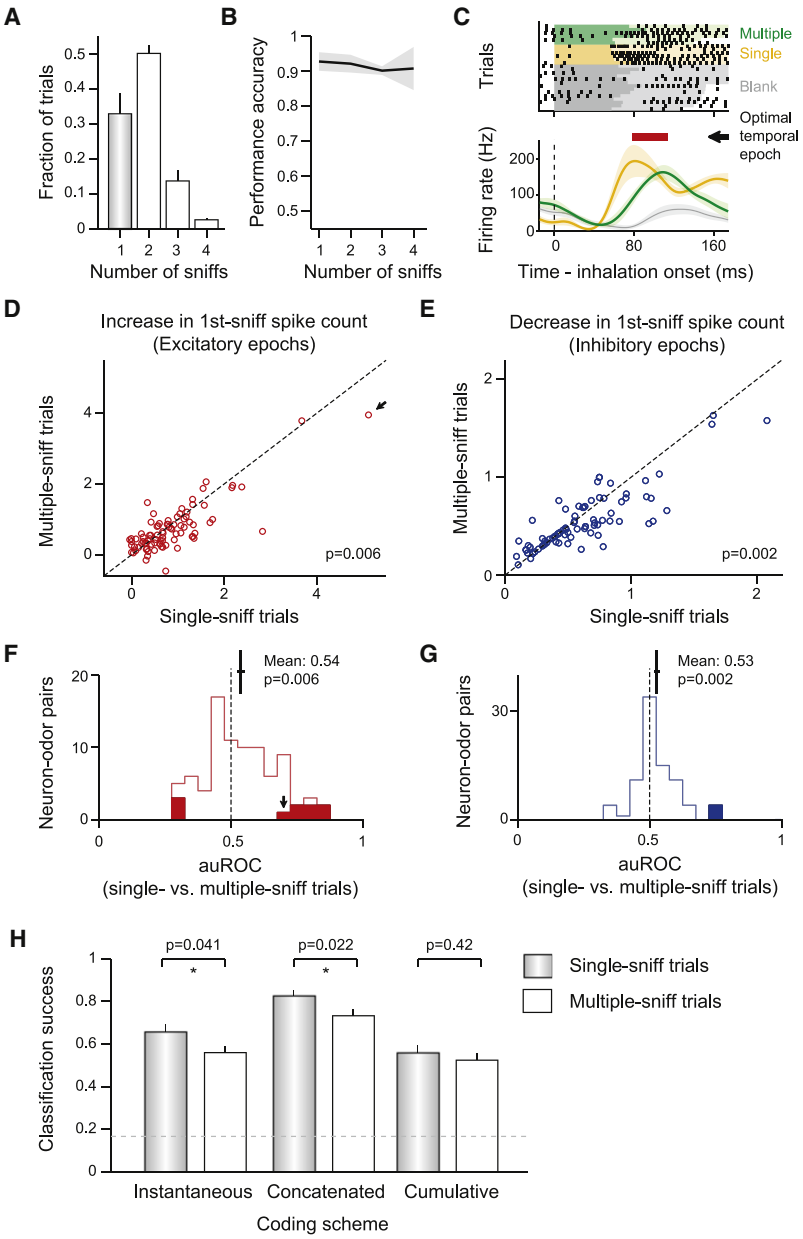

Figure 5. Subsniff Response Patterns Correlate with Behavioral Reaction Time during Odor Discrimination

(A) Number of sniffs taken during odor sampling (mean ± SD; n = 4 rats). Gray, single-sniff trials; white, multiple-sniff trials.

(B) Behavioral performance accuracy as a function of the number of sniffs (mean ± SD).

(C) The response of an example M/T cell to an odor for both single- and multiple-sniff trials, and to the blank control. Red bar: the optimal temporal epoch. PETHs are plotted as the mean ± SE.

(D and E) The magnitudes of first-sniff temporal responses are larger in single-sniff trials compared with those of multiple-sniff trials. The average change in spike count over the optimal temporal epoch, defined for each neuron-odor pair, is plotted for both excitatory (D) and inhibitory (E) epochs (n = 75 and 96 neuron-odor pairs, respectively). Each circle represents a neuron-odor pair, and the black arrow indicates the example pair in (C). Across the pool of neuron-odor pairs, responses were significantly larger in magnitude for single-sniff trials (one-tailed paired t test).

(F and G) Temporal response magnitudes correlate with behavioral reaction time on a trial-by-trial basis. The reliability with which single-sniff trials can be distinguished from multiple-sniff trials on a trial-by-trial basis was quantified using the ROC analysis. For inhibitory epochs, we defined an increased response magnitude as a reduction in spike count. Filled bars indicate individual responses that significantly differed from 0.5 ($p < 0.05$, z-test). Black arrow: the example response shown in (C). The mean and SE of auROC values across the pool of neuron-odor pairs is indicated by the cross (vertical and horizontal bars, respectively). This mean was significantly larger than 0.5 (one-tailed paired t test).

(H) First-sniff responses are more discriminable for single-sniff trials as compared with those of multiple-sniff trials when considering fine-scale activity. Classification analysis was performed as in Figure 3F (mean ± SE), but test data was composed of entirely single-sniff trials (gray bars) or multiple-sniff trials (white bars) over t = 0–120 ms following odor inhalation onset. Success rates were significantly higher for single-sniff trials when using instantaneous or concatenated coding schemes (*$p < 0.05$ for both schemes, χ^2 test over 200 repeats).

the scheme that was based on total spike counts ($p < 0.05$ for both instantaneous and concatenated schemes, $p > 0.4$ for cumulative scheme, χ^2 test over 200 repeats; Figure 5H). Taken together, these results strongly suggest that the activity of M/T cells within subsniff epochs, and not over more prolonged timescales, is read out by downstream brain centers to discriminate odors and guide behavior.

The Relationship between Respiration Frequency and Patterning of Spontaneous Activity

The above findings are inconsistent with previous sentiments that subsniff activity patterns of M/T cells do not play a major role in odor coding during rapid sniffing (Carey et al., 2009; Kay and Laurent, 1999). This view has been supported, in part, by reports that respiration-coupled patterning of M/T cell spontaneous activity, though widely observed during slow breathing or under anesthesia, appears much attenuated during this active mode of sampling (Bhalla and Bower, 1997; Kay and Laurent, 1999). We sought to clarify the relationship between respiration and spontaneous activity over a larger data set than has been previously described, which included 321 M/T cells recorded from seven animals. We identified periods throughout the recording session in which the animals were not engaged in a behavioral task (see Experimental Procedures). Figure 6A depicts a 7 s trace of a respiration measurement within one of these periods, demonstrating the range and complexity of

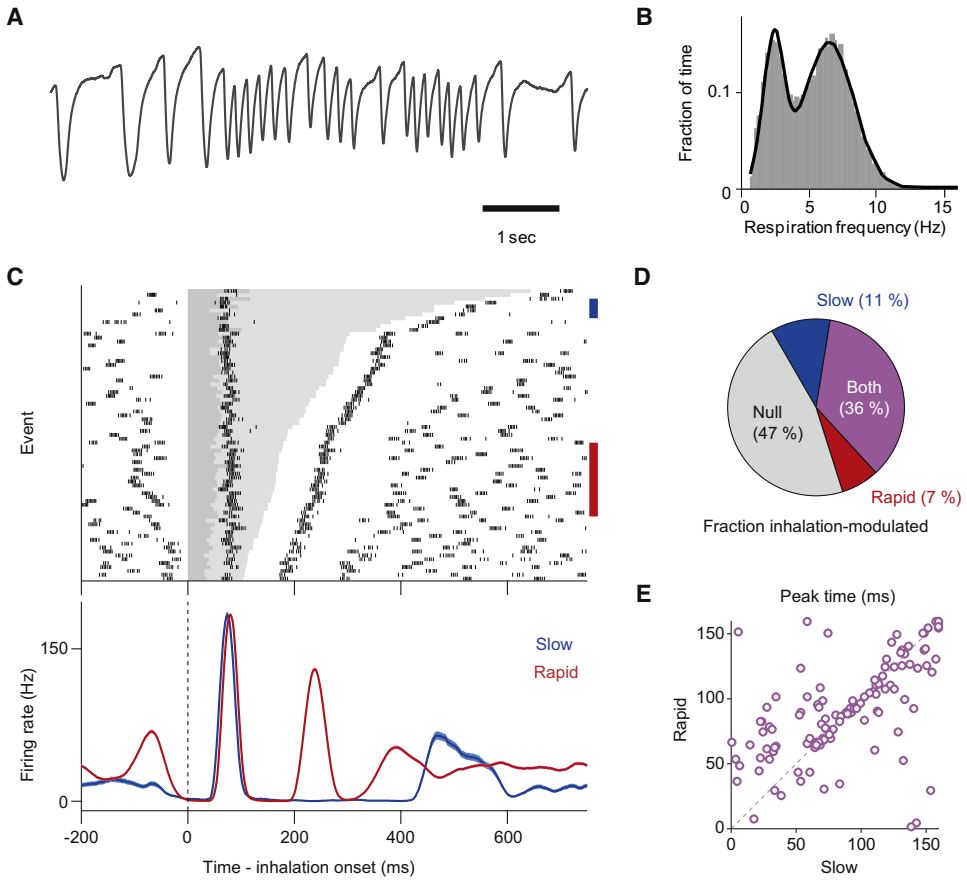

Figure 6. Inhalation-Coupled Modulation of Spontaneous Activity across Respiration Frequency

(A) Respiration behavior outside of task performance.

(B) Histogram of time spent at different respiration frequencies. The smooth black trace represents a Gaussian fit.

(C) Spontaneous activity of an example M/T cell aligned by inhalation onset. These plots are generated from respiration cycles occurring during periods outside of task performance, in the absence of odor stimulation. Top: raster plot sorted from top to bottom in terms of increasing respiration frequency. The colored bars on the right indicate the frequency ranges considered as slow breathing (blue, 2.32 ± 0.38 Hz, "slow," mean ± SD of the fitted Gaussian) and rapid sniffing (red, 6.40 ± 0.83 Hz, "rapid," mean ± SD of the fitted Gaussian). The gray shading indicates the first respiration cycle after inhalation onset, with the darker shading corresponding to the inhalation period. Bottom: PETHs for slow breathing (blue) and rapid sniffing (red) (mean ± SE).

(D) Fraction of M/T cells that showed significant inhalation-coupled modulation of spontaneous activity during slow breathing (blue) or rapid sniffing (red), with the overlap indicated in purple ("both") (n = 321 M/T cells; $p < 0.01$, χ^2 test).

(E) Comparison of the peak PETH timing between slow breathing and rapid sniffing. Only M/T cells that showed significant inhalation-coupled modulation in both conditions are plotted (n = 115 M/T cells).

natural respiration behavior. In total, this behavior was composed of two prominent modes: low-frequency respiration (2.32 ± 0.38 Hz, mean ± SD) reflecting slow breathing, and high-frequency respiration (6.40 ± 0.83 Hz, mean ± SD) characteristic of rapid sniffing (Figure 6B) (Welker, 1964; Youngentob et al., 1987).

To examine the relationship between respiration frequency and single-neuron spontaneous activity, we sorted individual respiration cycles according to their frequency and observed raster plots of corresponding spike trains aligned to the onset of inhalation (Figures 6C and S6). The activity patterns were quantified with PETHs for the ranges of respiration behavior characteristic of slow breathing and rapid sniffing. This analysis revealed a pronounced modulation of activity that is temporally coupled to inhalation onset and appears to be largely preserved across a wide range of respiration frequency. Overall, considering activity over the first 160 ms subsequent to inhalation, a large proportion of neurons exhibited significant modulation during both slow and rapid respiration behavior (47% and 43%, respectively; $p < 0.01$, χ^2 test against a flat PETH distribution; Figure 6D). Furthermore, the vast majority of modulated cells were modulated for both respiration conditions (36% of all cells).

To more explicitly characterize the nature of this preserved modulation, we compared the shapes of slow-breathing and rapid-sniffing PETHs. Because animals typically exhibit bouts of rapid sniffing, there appears to be some hysteresis in the spike patterning observed during high-frequency respiration as a result of activity driven by the previous sniff (Figures S6A and S6B). Nevertheless, basic temporal features, for example the peak

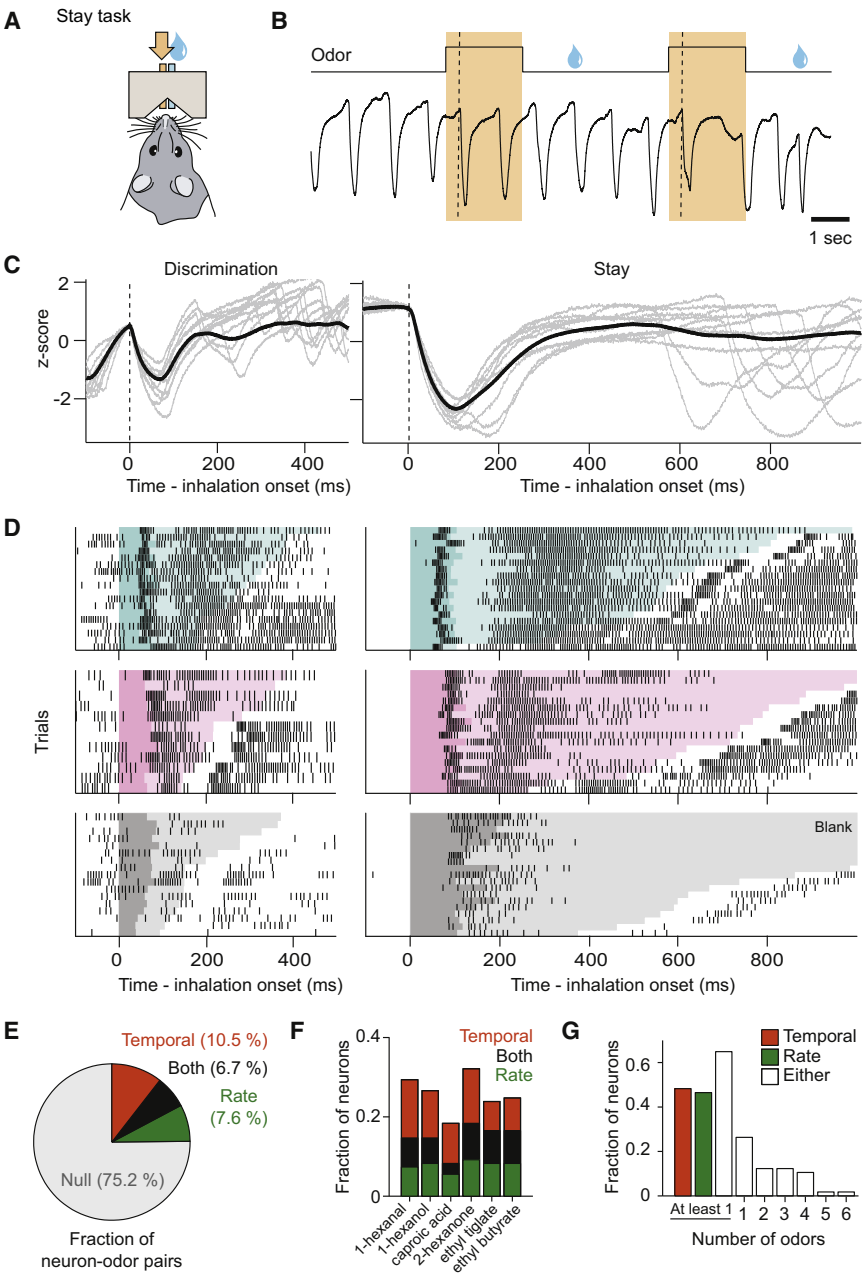

Figure 7. Odor Responses during Slow Breathing in the Stay Task

(A) The stay task.

(B) Task diagram (above) and respiration behavior (below).

(C) Comparison of respiration behavior during odor sampling between the discrimination task (left) and the stay task (right). Gray: 10 example traces. Black: the mean trace over all trials.

(D) Raster plots of the responses of an example M/T cell to two odors and the blank control (gray) in both the discrimination task (left) and stay task (right). Odors: blue, 2-hexanone; pink, 1-hexanol. Note the difference across tasks in spontaneous activity levels surrounding the onset of odor inhalation.

(E) Fraction of neuron-odor pairs that showed temporal (orange) or rate (green) responses, with the overlap indicated in black (both). Data are from 684 neuron-odor pairs (114 neurons, six odors).

(F) Per-stimulus fraction of neurons that showed temporal, rate, or both response types.

(G) Fraction of neurons that responded to at least one odor with a temporal response, with a rate response, or by either measure. Additionally plotted is the fraction that responded by either measure to a specific number of odors in the panel.

PETH timing, appear conserved across respiration conditions (pairwise correlation, R = 0.58; Figures 6E and S6).

Odor Responses during Slow Breathing

Are there features of the neural code for odor representations that are likewise conserved across changes in respiration frequency? To explicitly address this question, we devised a task in which rats were exposed to odors during slow breathing (a "stay" task). The animals were trained to maintain their snout in a port outfitted for both water and odor delivery (Figure 7A and 7B; see Experimental Procedures). A water reward was delivered when the animal stayed in the port for five to six consecutive seconds, and interleaved between rewards, a two second odor pulse was delivered. Rats typically expressed low-frequency breathing throughout the period in which they stayed in the port, even in the presence of an odor (Figures 7B, 7C, and S7). Additionally, both the duration and amplitude of inhalation were dramatically increased in comparison to the discrimination task (median inhalation duration, 180 ± 64 ms versus 70 ± 5 ms; median inhalation amplitude, 2.2 ± 0.4 versus 1.7 ± 0.1, in terms of z-score; mean ± SD; Figure S7). We trained animals on this task in addition to the discrimination task, and they performed both tasks back to back in a given recording session, each utilizing the same panel of six odors (n = 3 animals; 101 M/T cells recorded in both tasks). This allowed us to make direct comparisons between odor responses of the same cells to the same odors across widely divergent respiration behaviors (Figure 7D). During slow breathing of an odor, we identified both rate and temporal responses (14% and 17% of neuron-odor pairs, respectively) when considering only the first 160 ms following inhalation onset (Figures 7E and 7F), with 65% of neurons responding to at least one odorant by either measure (Figure 7G).

We next compared the M/T cell population response dynamics between the two tasks. Figure 8A depicts the interodor distance between mean population responses within each task. Maximum

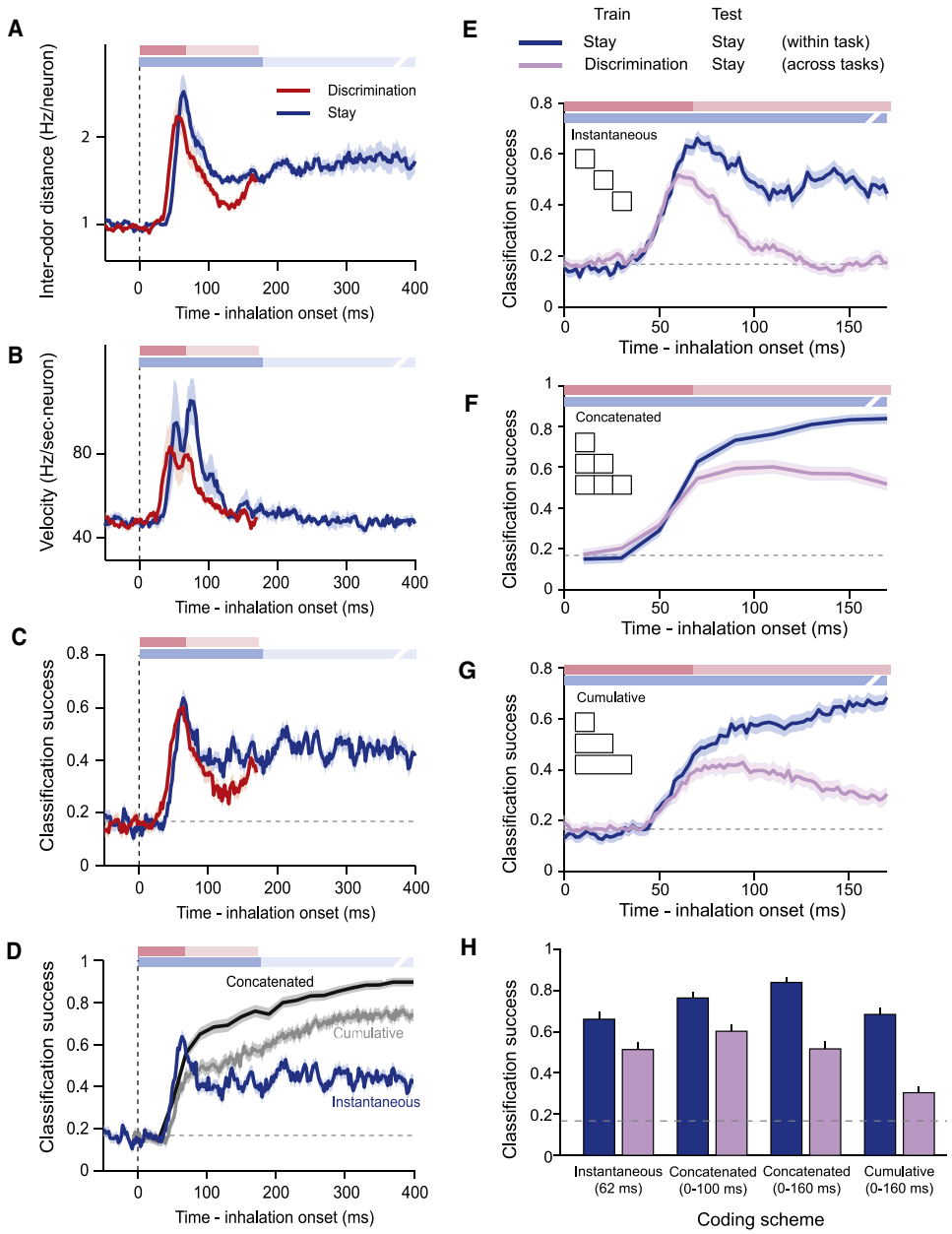

Figure 8. Initial Portions of Transient Response Are Highly Conserved between Rapid Sniffing and Slow Breathing

(A) Distance between M/T cell population responses during rapid sniffing (discrimination task, red) and slow breathing (stay task, blue). Both traces were computed over the same M/T cell population (n = 85 M/T cells, used for A–D; mean ± SE). The red and blue shaded bars at the top detail the median respiration behavior for rapid sniffing and slow breathing, respectively, with the darker shading indicating the inhalation period, and the lighter shading indicating total respiration duration (though truncated at 400 ms).

(B) Rate of change (velocity) of M/T cell population responses (mean ± SE).

(C) Time course of the performance of a linear classifier based on instantaneous activity patterns (plotted as mean ± SE in this and all subsequent panels).

(D) Comparison of the classification performance for slow breathing responses across three different coding schemes.

(E) Comparison of the performance of linear classifier based on instantaneous activity patterns (see schematic at inset) of an M/T cell population (n = 101 M/T cells, used for plots E–H) within and across the two tasks. Blue, a linear classifier was trained and tested using slow breathing data from the stay task, as in (C); purple, a linear classifier was trained using rapid sniffing data from the discrimination task, and tested using slow breathing data from the stay task.

(F) Comparison of the performance of classifiers based on concatenated bins within and across the two tasks.

(G) Comparison of the performance of classifiers based on cumulative spike counts within and across the two tasks.

(H) Summary of performance of the different coding schemes detailed in (E)–(G).

separation was observed shortly after inhalation onset in both tasks, as both measures peaked after ~60 ms. It is interesting to note that the initial response exhibits a similar time course in both conditions despite dramatic differences in inhalation behavior (e.g., inhalation duration). Slow breathing responses do not continue to become more separated despite prolonged stimulus input, but rather begin to decay amidst inhalation, ultimately settling at an intermediate level of separation that is maintained throughout the prolonged exhalation. Similarly, the rate of change of the population response for slow breathing resembles that of rapid sniffing over the first ~100 ms, reaching a maximum shortly after the onset of inhalation (Figure 8B). Around the end of inhalation, this velocity has nearly returned to baseline levels, and eventually does so after ~200 ms. These observations indicate that the first inhalation of an odor generally induces a rapidly fluctuating and highly separated population response that unfolds over a timescale that approximates a rapid sniff cycle. These inhalation-coupled response dynamics appear invariant to changes in the duration and amplitude of inhalation, and also to the overall frequency of respiration.

Given these commonalities, we suspected that the best coding strategy for discriminating slow-breathing population responses would also rely on fine-scale activity, particularly over the early inhalation-coupled period. To test this, we applied a linear classification method (as in Figure 4F) to evaluate the discriminability of slow breathing responses over the 400 ms following inhalation onset. Using a coding scheme based on activity within instantaneous 20 ms epochs, success rates reached a maximum at ~60 ms, and were significantly higher during the rapidly fluctuating, inhalation-coupled period as compared with those of the later, steadier response (Figure 8C, blue trace). Furthermore, a code based on the concatenation of activity over consecutive epochs further improved discrimination, as success rates rapidly increased over the first 160 ms (Figure 8D). Finally, the performance of a simple integrator of cumulative spike counts exhibited similar characteristics to those of the concatenated scheme, though with significantly lower overall success throughout the response. In total, aspects of the neural code for odor representations during slow breathing appear to be consistent with that of rapid sniffing, with the bulk of stimulus information conveyed by the fine-scale temporal spike patterning that is tightly coupled to the onset of inhalation.

Temporal Code Based on Initial Transient Response Is Conserved between Rapid Sniffing and Slow Breathing

More direct evidence for the conservation of a coding scheme would be reflected in the ability of a single classifier to discriminate responses from both tasks. We explicitly tested this by comparing the efficacy of a linear classifier trained on rapid sniffing responses (discrimination task) to discriminate slow breathing responses (stay task) (Figures 8E–8H, purple plots) (Bathellier et al., 2008; Brown et al., 2005). The three coding schemes tested were the same as detailed above. We considered only the first 160 ms following the first odor inhalation onset, and contrasted these results with the performance of a classifier that was both trained and tested on slow breathing responses (Figures 8E–8H, blue plots). Our results for the instantaneous coding scheme are shown in Figure 8E. We observed that success rates were closely matched over the earliest epochs of the response, up to ~60 ms following inhalation onset. However, subsequent to this, classifying across tasks quickly degraded, reaching chance levels by ~140 ms. This result demonstrates that fine-scale activity patterns over the initial portions of odor responses are highly conserved between rapid sniffing and slow breathing.

The degraded performance observed in the later epochs of the response has negative implications as to the capacity of a classifier based on concatenated time bins to discriminate across tasks: classification success is slightly improved above the peak instantaneous result over the first ~100 ms, whereupon incorporating additional epochs actually hinders the performance (Figure 8F). This means that a coding scheme based on the patterned spiking activity over the entire duration of a sniff is not ideal for discriminating across respiration modes. Finally, coding based on cumulative spike counts exhibits the poorest performance, particularly as the integration window was expanded beyond the early portion of the response (Figure 8G). These results demonstrate that a coding scheme based on fine-scale temporal features over the initial transient response, up to ~100 ms following inhalation, forms a robust code that is largely conserved across changes in respiration frequency (Figure 8H).

DISCUSSION

We found that coding schemes based on the subsniff timing of spikes are the most likely candidates for the representation of odor identity by the mammalian OB. Our main findings in support of this are as follows. (1) We demonstrated that the first inhalation of an odor triggered reliable cell- and odor-specific spike patterns within a sniff. (2) These patterns conveyed substantial odor information over the first 100 ms following inhalation. (3) Temporally modulated responses correlated with behavioral discrimination time on a trial-by-trial basis. (4) The initial transient portions of odor-evoked patterns were highly preserved between rapid sniffing and slow breathing. Finally, (5) slower features of the response (total spike count over a respiration cycle) carried less odor information, did not correlate with behavior, and were poorly conserved across respiration modes.

Our results are in stark contrast with previous proposals that have argued against a role for subsniff temporal coding by M/T cells. A few key experimental distinctions between our study and previous works likely account for this inconsistency. First, our experiments were done in awake animals, and conclusions made under anesthesia may be confounded by the rather significant impact that anesthetics have on baseline activity and odor responsivity in the OB (e.g., Adrian, 1950; Rinberg et al., 2006a). These factors may have contributed to the observations made in a recent report in anesthetized mice, where temporal responses rarely occurred in the absence of a significant change in overall firing rate, exhibited rather homogenous timing, and ultimately contributed very little to classification accuracy over the performance achieved using total spike counts (Bathellier et al., 2008). Second, while previous studies in awake animals proposed that activity becomes uncoupled from respiration during rapid sniffing and that odor responses become more variable, they did not explicitly measure the respiration rhythm (Kay and

Laurent, 1999), or did so in the absence of a controlled stimulus delivery (Bhalla and Bower, 1997). Accounting for these factors allowed for the precise identification of the first inhalation of the odorant in our study. Ultimately, our results stress the necessity of monitoring M/T cell spike trains at a resolution of tens of milliseconds with respect to inhalation onset.

Coding mechanisms that utilize the timing of spikes have been proposed to garner computational advantages over those based on the total spike count. These advantages include the ability to encode complex stimulus patterns within a short period of time (Gollisch and Meister, 2008; Hopfield, 1995; Schaefer and Margrie, 2007; Thorpe et al., 2001; Uchida and Mainen, 2003), and to provide "extra bandwidth" for encoding more information (Laurent, 1999; Schaefer and Margrie, 2007; Wehr and Laurent, 1996). Our data are in agreement with both of these proposals. It is of interest to note that the relatively high spontaneous firing rates of M/T cells in awake animals appear to reduce the utility of simpler coding mechanisms based on spike latency (i.e., timing of first spike; Figure S4D). Furthermore, normalizing spike times by their phase within the respiration cycle reduces discrimination accuracy (Figure S4D).

M/T cell odor responses were diverse in terms of the timing and magnitude of activity within a single sniff. Collectively, these responses form odor-specific spatio-temporal patterns that (1) rapidly fluctuate over the course of the respiration cycle and (2) contain substantial odor information over fine timescales. Similar response dynamics have been observed for neural populations within the locust antennae lobe over the first 1–2 s of a prolonged odor pulse (Mazor and Laurent, 2005). In that study, this aspect of the response was found to be more discriminable as compared with later stages wherein the responses were shown to reach a more stable state. While our results are consistent with these observations, it is interesting to note that the rate of change observed in our population response data was faster than has been described in the locust (Brown et al., 2005; Mazor and Laurent, 2005; Stopfer et al., 2003), or in anesthetized mice (Bathellier et al., 2008). We observed that instantaneous odor representations became substantially independent over the course of 30–40 ms, and therefore odor information could be accumulated over subsequent time points within a single rapid sniff cycle. Considering that we observed this high-velocity, inhalation-coupled response even during slow breathing, it may reflect fundamental features of the OB circuitry that are tuned to the upper bounds of the rate of natural sampling behavior (i.e., rapid sniffing).

The ultimate test of the relevance of a given neural code is whether it is utilized by downstream brain centers to guide stimulus-appropriate behavioral responses. We demonstrated that subsniff temporal activity of M/T cell responses, and not their total spike count, correlates with variability in behavioral discrimination time. This strongly suggests that these fine-scale activity patterns represent the neural code that communicates the identity of an odor to downstream brain centers. Correlations between trial-to-trial variability of neural activity and behavioral performance have been used to establish the relevant features of neural responses in the visual system (Parker and Newsome, 1998), though to our knowledge, our study is the first to apply such an approach to the olfactory system. Our finding is compatible with various types of decision models that posit that a decision is made when the animal has obtained sufficient sensory evidence. These include integrator models (which accumulate sensory evidence over extended periods of time; i.e., across multiple sniffs) (Gold and Shadlen, 2007; Smith and Ratcliff, 2004) and probability summation models (which use only recently obtained evidence; i.e., the most recent sniff) (Watson, 1979). Our preliminary analysis of the discriminability of responses within and across sniffs of double-sniff trials does not sufficiently distinguish between these models because they both can support our behavioral observation that performance is equivalent between single- and multiple-sniff trials, depending on the coding scheme used for classification (Figure S5O). Future experiments will be necessary to fully clarify the relevance of these models. For example, in certain task conditions, it has been suggested that animals prolong odor sampling, presumably accumulating evidence over multiple sniffs, to improve odor representations (Abraham et al., 2004; Rinberg et al., 2006b). The use of more challenging stimulus conditions (e.g., binary odor mixtures) will be critical in determining which of these models holds up at the psychophysical limit.

We found that the initial transient portions of odor responses were highly conserved across distinct modes of sampling, whereas slower features such as the total spike count were not. This is consistent with recent theoretical studies that proposed that rapidly fluctuating response dynamics can provide a basis for information coding that is robust to various perturbations (e.g., noise, or differences in initial conditions) (Moazzezi and Dayan, 2008; Rabinovich et al., 2008). Indeed, numerous behavioral and neurophysiological features deviated between our two behavioral tasks, which would appear to pose challenges to such a conserved neural code. (1) In addition to the change in respiration frequency, inhalation parameters (amplitude and duration) differed quite dramatically and are known to influence the interaction of odorants with the olfactory mucosa (Mainland and Sobel, 2006; Oka et al., 2009; Schoenfeld and Cleland, 2006; Scott, 2006). Furthermore, (2) owing to a pronounced modulation of spontaneous activity that was tightly coupled to inhalation, we observed hysteresis of activity patterns when inhalations occurred in short succession (e.g., during a bout of rapid sniffing), which could potentially impact the initial response. Finally, (3) the odors were sampled in different behavioral contexts, and factors such as reward expectation, motor behavior, and attention have been described to substantially modulate the activity of M/T cells (Doucette and Restrepo, 2008; Kay and Laurent, 1999). While we cannot speak to the underlying mechanisms, we do observe such modulation in our data (see Figure 1C, bottom trace). Our finding that the initial response was conserved even in the face of all these complexities suggests that the initial transient portions of odor responses represent a particularly robust code that can be utilized to recognize odors across diverse behavioral contexts (e.g., between active and restful states), which represents a form of perceptual constancy. A previous study in the locust antenna lobe described a similar conservation of the initial response across repeated brief odor pulses like those that are encountered in natural odor plumes, even in conditions that resulted in overlapping responses across subsequent odor

presentations (Brown et al., 2005). Together, these findings suggest that common strategies for the invariant coding of odors during dynamic sampling conditions may exist across diverse animal species. Additionally, considering that the later portions of responses contain differing odor information between rapid sniffing and slow breathing, our data provide some evidence that modulating respiration behavior may enable the animal to exert control over the nature of the olfactory information that is obtained (Mainland and Sobel, 2006; Youngentob et al., 1987).

Because rapid sniffing is typically observed during exploratory and attentive states (Welker, 1964), it is believed in some way to facilitate sensory processing. However, by our measures, the discriminability of M/T cell spike trains was not improved during rapid sniffing (e.g., Figure 8C). This raises the question as to why animals sniff rapidly under certain conditions (Verhagen et al., 2007; Wesson et al., 2009). One explanation is that rapid sniffing maximizes the number of information-rich neural transients that can be obtained per unit time, which would be of particular utility considering the patchily distributed nature of odor plumes. Thus, rapid sampling behavior may be crucial for efficiently determining where and when relevant odor cues are encountered in order to enact timely and appropriate behavioral responses. While our study provides behavioral evidence that strongly suggests that mammals actually use inhalation-coupled temporal responses to guide behavior, it will be the task of future studies to determine which neurons read out these temporal patterns, the mechanisms by which this readout is accomplished, and ultimately how this activity is transformed into a behavioral response. Approaches that combine psychophysical behavioral experiments with recordings in olfactory areas downstream of the OB will be crucial toward this effort.

EXPERIMENTAL PROCEDURES

See Supplemental Information for detailed procedures. All procedures involving animals were carried out in accordance with NIH standards and approved by the Harvard University Institutional Animal Care and Use Committee (IACUC). All values were represented by the mean ± standard error (SE) unless otherwise noted.

Behavioral Paradigms

In total, eight Long Evans rats were used. For a given session, rats performed one or both behavioral tasks (discrimination and stay tasks) to obtain water rewards. In the discrimination task, rats were trained to discriminate a panel of six odorants for water rewards (n = 5 rats; 52 sessions, 176 ± 65 trials/session; mean ± SD) as was described in Uchida and Mainen (2003). In addition, to obtain a measure of baseline activity during odor sampling, we introduced blank trials in which no odor stimulus was delivered while the rat was rewarded randomly for choices to either port (reward probability: 0.75).

In order to examine odor responses during slow breathing, we devised a stay task (n = 3 rats; 29 sessions with both discrimination and stay tasks performed, 149 ± 20 and 139 ± 54 trials/session, respectively; mean ± SD). Animals were trained to maintain their snout in a central port outfitted for both water and odor delivery. A 2 s odor pulse was initiated after the rat stayed in the port for 3 s, with water reward being delivered 1 s after the termination of odor. Thereafter, if the animal maintained its snout in the port, the sequence repeated with the next odor delivery occurring 2 s after the delivery of water.

Odor Stimuli

Odor delivery was controlled by a custom-made olfactometer as described previously (Uchida and Mainen, 2003). Odors were delivered at 0.05% of saturated vapor, achieved by first diluting an odor in paraffin oil 1:100, and further diluting 50 ml/min odorized air into a 950 ml/min clean air stream upon delivery. For blank control trials, the air stream was diverted through a filter containing no odorants. Both tasks were conducted using a standardized panel of six odors: 1-hexanal, 1-hexanol, caproic acid, 2-hexanone, ethyl tiglate, and ethyl butyrate.

Neural and Respiration Recordings

Upon completion of behavioral training, rats were implanted with a custom-made multielectrode drive (Feierstein et al., 2006; Kepecs et al., 2008) with 6 or 12 independently adjustable tetrodes above the OB under anesthesia (ketamine/medetomidine, 60/0.5 mg/kg, i.p.). To monitor respiration behavior, a thermocouple was implanted into the nasal cavity ipsilateral to the recording site (Uchida and Mainen, 2003). Recordings were obtained over 2–4 weeks, with electrode depths adjusted prior to each behavioral session. Data acquisition was performed using the DigiLynx system (Neuralynx, Tucson, AZ), and was synchronized with behavioral data by acquiring TTL pulses of task performance.

Individual electrode data were filtered between 600 and 6000 Hz and digitized at 32 kHz. Spikes were collected as 1 ms waveforms triggered online by a manually set threshold. For each tetrode, single units were isolated offline by manually clustering spike features using MClust software in MATLAB (written by A.D. Redish; Figure S1). For more details on our identification of neuron types, see Supplemental Experimental Procedures.

Statistical Analysis of Single Neurons

In total, we recorded from 432 single neurons. Within this data set, 232 neurons were recorded in the discrimination task that constitutes the main data set. Furthermore, 101 out of these 232 neurons were recorded in both the discrimination and stay tasks. We used a nonparametric test, the Wilcoxon rank sum test, to identify significant changes in the total spike count (rate responses; Figure 1E). Significant changes in the temporal distribution of spikes were identified using the Kolmogorov-Smirnov test (temporal responses). For the analysis of spontaneous activity, we compared inhalation-coupled modulation over an equivalent window of time (0–160 ms following inhalation onset) between rapid sniffing and slow breathing, using the χ^2 test. PETHs (eight 20 ms nonoverlapping bins) were compared against a uniform histogram distribution with a matched mean.

Identification of the Optimal Temporal Response Epoch

In order to quantify the reliability, sign (excitatory or inhibitory), and timing of temporal responses over subsniff epochs, we used a method based on signal detection theory (Green and Swets, 1966; Stüttgen and Schwarz, 2008). For a given neuron-odor pair, single-trial spike count distributions were compared between odor and blank responses within a matched temporal epoch using the area under the ROC curve (auROC). The epoch size and position were incrementally varied (5–160 ms bin size; 0–160 ms bin center position, relative to the first odor inhalation onset), and the combination that produced the maximum discriminability (max $|\text{auROC} - 0.5|$) between the two distributions was identified as the optimal response epoch.

Population Vector Construction and Analysis

Instantaneous population activity was represented as an n dimensional vector whose nth element was the mean spike count of the nth neuron over a given 20 ms bin. The distance between odor representations was computed as the Euclidean distance between pairs of activity vectors at a given instant. The velocity of population responses was determined as the distance between successive, nonoverlapping 20 ms bins.

Classification Success Analysis

Classification analysis was performed using a support vector machine (SVM) algorithm with a linear kernel (Hung et al., 2005). Analysis was conducted on trial data pooled across all recording sessions. Input to the algorithm consisted of activity vectors derived from single-trial responses, where the length of the vector was determined by the number of neurons times the number of time bins. To compute classification success, generally, one trial per stimulus was chosen as a test set, and the remaining trials were used to train the algorithm. The success rate was defined as the fraction of test trials that were

correctly identified. For statistical analysis, see Supplemental Experimental Procedures.

For classification success of instantaneous time points, testing was done using activity vectors derived from the same time, t_i, as the training set (20 ms window, $t_i \pm 10$ ms, stepped in 2 ms increments; e.g., Figure 4D), or with a temporal offset (Figures 4E and S4A). For classification based on concatenated bins, activity vectors were obtained from a series of nonoverlapping time bins (20 ms bins; e.g., for $t_i = 50$ ms, input consists of three bins, centered at 10, 30, and 50 ms; e.g., Figure 4F, black trace). Finally, activity vectors for the analysis of cumulative spike counts were constructed by summing the total spikes between t = 0 and t = t_i + 10 ms.

Correlation between Neural Activity and Behavioral Reaction Time

For this analysis, we included data from four rats performing the reaction time version of the discrimination task. Single-cell analysis was performed separately for temporal responses (171 neuron-odor pairs; Figures 5D–5G) and rate responses (171 neuron-odor pairs; Figures S5A–S5D). Temporal responses were analyzed over an optimal temporal epoch that was identified for each response as described above, with the restriction that the epoch bounds could not exceed 0–120 ms. Rate responses were analyzed over the entire 0–120 ms window.

SUPPLEMENTAL INFORMATION

Supplemental Information for this article includes seven figures, Supplemental Experimental Procedures, and two videos and can be found with this article online at doi:10.1016/j.neuron.2010.09.040.

ACKNOWLEDGMENTS

We thank John Assad, Kenny Blum, Katherine Gaudry, Rafi Haddad, Gabriel Kreiman, Zachary Mainen, Ofer Mazor, Markus Meister, Keiji Miura, Venkatesh Murthy, Tomokazu Sato, Gary Sing, Rachel Wilson, Alice Wang, and other members of the Uchida lab for valuable comments and discussions. We are grateful to Ed Soucy for technical support. This work was supported by the Smith Family Young Investigator Award, Milton Fund, and Alfred Sloan Foundation, and startup funding from Harvard University.

Accepted: September 27, 2010
Published: November 3, 2010

REFERENCES

Abraham, N.M., Spors, H., Carleton, A., Margrie, T.W., Kuner, T., and Schaefer, A.T. (2004). Maintaining accuracy at the expense of speed: Stimulus similarity defines odor discrimination time in mice. Neuron *44*, 865–876.

Adrian, E.D. (1950). The electrical activity of the mammalian olfactory bulb. Electroencephalogr. Clin. Neurophysiol. *2*, 377–388.

Bathellier, B., Buhl, D.L., Accolla, R., and Carleton, A. (2008). Dynamic ensemble odor coding in the mammalian olfactory bulb: Sensory information at different timescales. Neuron *57*, 586–598.

Bhalla, U.S., and Bower, J.M. (1997). Multiday recordings from olfactory bulb neurons in awake freely moving rats: Spatially and temporally organized variability in odorant response properties. J. Comput. Neurosci. *4*, 221–256.

Britten, K.H., Newsome, W.T., Shadlen, M.N., Celebrini, S., and Movshon, J.A. (1996). A relationship between behavioral choice and the visual responses of neurons in macaque MT. Vis. Neurosci. *13*, 87–100.

Brown, S.L., Joseph, J., and Stopfer, M. (2005). Encoding a temporally structured stimulus with a temporally structured neural representation. Nat. Neurosci. *8*, 1568–1576.

Cang, J., and Isaacson, J.S. (2003). In vivo whole-cell recording of odor-evoked synaptic transmission in the rat olfactory bulb. J. Neurosci. *23*, 4108–4116.

Carey, R.M., Verhagen, J.V., Wesson, D.W., Pírez, N., and Wachowiak, M. (2009). Temporal structure of receptor neuron input to the olfactory bulb imaged in behaving rats. J. Neurophysiol. *101*, 1073–1088.

Chaput, M.A. (1986). Respiratory-phase-related coding of olfactory information in the olfactory bulb of awake freely-breathing rabbits. Physiol. Behav. *36*, 319–324.

Cohen, M.R., and Newsome, W.T. (2009). Estimates of the contribution of single neurons to perception depend on timescale and noise correlation. J. Neurosci. *29*, 6635–6648.

Doucette, W., and Restrepo, D. (2008). Profound context-dependent plasticity of mitral cell responses in olfactory bulb. PLoS Biol. *6*, e258.

Fantana, A.L., Soucy, E.R., and Meister, M. (2008). Rat olfactory bulb mitral cells receive sparse glomerular inputs. Neuron *59*, 802–814.

Feierstein, C.E., Quirk, M.C., Uchida, N., Sosulski, D.L., and Mainen, Z.F. (2006). Representation of spatial goals in rat orbitofrontal cortex. Neuron *51*, 495–507.

Friedrich, R.W., and Laurent, G. (2001). Dynamic optimization of odor representations by slow temporal patterning of mitral cell activity. Science *291*, 889–894.

Friedrich, R.W., and Stopfer, M. (2001). Recent dynamics in olfactory population coding. Curr. Opin. Neurobiol. *11*, 468–474.

Gold, J.I., and Shadlen, M.N. (2007). The neural basis of decision making. Annu. Rev. Neurosci. *30*, 535–574.

Gollisch, T., and Meister, M. (2008). Rapid neural coding in the retina with relative spike latencies. Science *319*, 1108–1111.

Green, D.M., and Swets, J.A. (1966). Signal Detection Theory and Psychophysics (New York: Wiley).

Hamilton, K.A., and Kauer, J.S. (1989). Patterns of intracellular potentials in salamander mitral/tufted cells in response to odor stimulation. J. Neurophysiol. *62*, 609–625.

Hopfield, J.J. (1995). Pattern recognition computation using action potential timing for stimulus representation. Nature *376*, 33–36.

Hung, C.P., Kreiman, G., Poggio, T., and DiCarlo, J.J. (2005). Fast readout of object identity from macaque inferior temporal cortex. Science *310*, 863–866.

Karpov, A.P. (1980). Analysis of neuron activity in the rabbit's olfactory bulb during food-acquisition behavior. In Neural Mechanisms of Goal-Directed Behavior, R.F. Thompson, L.H. Hicks, and V.B. Shvyrkov, eds. (New York: Academic Press), pp. 273–282.

Kay, L.M., and Laurent, G. (1999). Odor- and context-dependent modulation of mitral cell activity in behaving rats. Nat. Neurosci. *2*, 1003–1009.

Kepecs, A., Uchida, N., and Mainen, Z.F. (2006). The sniff as a unit of olfactory processing. Chem. Senses *31*, 167–179.

Kepecs, A., Uchida, N., and Mainen, Z.F. (2007). Rapid and precise control of sniffing during olfactory discrimination in rats. J. Neurophysiol. *98*, 205–213.

Kepecs, A., Uchida, N., Zariwala, H.A., and Mainen, Z.F. (2008). Neural correlates, computation and behavioural impact of decision confidence. Nature *455*, 227–231.

Laurent, G. (1999). A systems perspective on early olfactory coding. Science *286*, 723–728.

Luce, R.D. (1986). Response Times: Their Role in Inferring Elementary Mental Organization (New York: Oxford Univ Press).

Luna, R., Hernández, A., Brody, C.D., and Romo, R. (2005). Neural codes for perceptual discrimination in primary somatosensory cortex. Nat. Neurosci. *8*, 1210–1219.

Macrides, F., and Chorover, S.L. (1972). Olfactory bulb units: Activity correlated with inhalation cycles and odor quality. Science *175*, 84–87.

Mainen, Z.F. (2006). Behavioral analysis of olfactory coding and computation in rodents. Curr. Opin. Neurobiol. *16*, 429–434.

Mainland, J., and Sobel, N. (2006). The sniff is part of the olfactory percept. Chem. Senses *31*, 181–196.

Margrie, T.W., and Schaefer, A.T. (2003). Theta oscillation coupled spike latencies yield computational vigour in a mammalian sensory system. J. Physiol. *546*, 363–374.

Mazor, O., and Laurent, G. (2005). Transient dynamics versus fixed points in odor representations by locust antennal lobe projection neurons. Neuron *48*, 661–673.

Meredith, M. (1986). Patterned response to odor in mammalian olfactory bulb: The influence of intensity. J. Neurophysiol. *56*, 572–597.

Meredith, M., and Moulton, D.G. (1978). Patterned response to odor in single neurones of goldfish olfactory bulb: Influence of odor quality and other stimulus parameters. J. Gen. Physiol. *71*, 615–643.

Moazzezi, R., and Dayan, P. (2008). Change-based inference for invariant discrimination. Network *19*, 236–252.

Oka, Y., Takai, Y., and Touhara, K. (2009). Nasal airflow rate affects the sensitivity and pattern of glomerular odorant responses in the mouse olfactory bulb. J. Neurosci. *29*, 12070–12078.

Parker, A.J., and Newsome, W.T. (1998). Sense and the single neuron: Probing the physiology of perception. Annu. Rev. Neurosci. *21*, 227–277.

Rabinovich, M., Huerta, R., and Laurent, G. (2008). Neuroscience. Transient dynamics for neural processing. Science *321*, 48–50.

Rajan, R., Clement, J.P., and Bhalla, U.S. (2006). Rats smell in stereo. Science *311*, 666–670.

Rinberg, D., and Gelperin, A. (2006). Olfactory neuronal dynamics in behaving animals. Semin. Cell Dev. Biol. *17*, 454–461.

Rinberg, D., Koulakov, A., and Gelperin, A. (2006a). Sparse odor coding in awake behaving mice. J. Neurosci. *26*, 8857–8865.

Rinberg, D., Koulakov, A., and Gelperin, A. (2006b). Speed-accuracy tradeoff in olfaction. Neuron *51*, 351–358.

Schaefer, A.T., and Margrie, T.W. (2007). Spatiotemporal representations in the olfactory system. Trends Neurosci. *30*, 92–100.

Schoenfeld, T.A., and Cleland, T.A. (2006). Anatomical contributions to odorant sampling and representation in rodents: Zoning in on sniffing behavior. Chem. Senses *31*, 131–144.

Scott, J.W. (2006). Sniffing and spatiotemporal coding in olfaction. Chem. Senses *31*, 119–130.

Smith, P.L., and Ratcliff, R. (2004). Psychology and neurobiology of simple decisions. Trends Neurosci. *27*, 161–168.

Spors, H., and Grinvald, A. (2002). Spatio-temporal dynamics of odor representations in the mammalian olfactory bulb. Neuron *34*, 301–315.

Stopfer, M., Jayaraman, V., and Laurent, G. (2003). Intensity versus identity coding in an olfactory system. Neuron *39*, 991–1004.

Stüttgen, M.C., and Schwarz, C. (2008). Psychophysical and neurometric detection performance under stimulus uncertainty. Nat. Neurosci. *11*, 1091–1099.

Thorpe, S., Delorme, A., and Van Rullen, R. (2001). Spike-based strategies for rapid processing. Neural Netw. *14*, 715–725.

Uchida, N., and Mainen, Z.F. (2003). Speed and accuracy of olfactory discrimination in the rat. Nat. Neurosci. *6*, 1224–1229.

Verhagen, J.V., Wesson, D.W., Netoff, T.I., White, J.A., and Wachowiak, M. (2007). Sniffing controls an adaptive filter of sensory input to the olfactory bulb. Nat. Neurosci. *10*, 631–639.

Watson, A.B. (1979). Probability summation over time. Vision Res. *19*, 515–522.

Wehr, M., and Laurent, G. (1996). Odour encoding by temporal sequences of firing in oscillating neural assemblies. Nature *384*, 162–166.

Welker, W.I. (1964). Analysis of sniffing of the albino rat. Behaviour *22*, 223–244.

Wellis, D.P., Scott, J.W., and Harrison, T.A. (1989). Discrimination among odorants by single neurons of the rat olfactory bulb. J. Neurophysiol. *61*, 1161–1177.

Wesson, D.W., Carey, R.M., Verhagen, J.V., and Wachowiak, M. (2008a). Rapid encoding and perception of novel odors in the rat. PLoS Biol. *6*, e82.

Wesson, D.W., Donahou, T.N., Johnson, M.O., and Wachowiak, M. (2008b). Sniffing behavior of mice during performance in odor-guided tasks. Chem. Senses *33*, 581–596.

Wesson, D.W., Verhagen, J.V., and Wachowiak, M. (2009). Why sniff fast? The relationship between sniff frequency, odor discrimination, and receptor neuron activation in the rat. J. Neurophysiol. *101*, 1089–1102.

Wilson, R.I. (2008). Neural and behavioral mechanisms of olfactory perception. Curr. Opin. Neurobiol. *18*, 408–412.

Wilson, R.I., and Mainen, Z.F. (2006). Early events in olfactory processing. Annu. Rev. Neurosci. *29*, 163–201.

Youngentob, S.L., Mozell, M.M., Sheehe, P.R., and Hornung, D.E. (1987). A quantitative analysis of sniffing strategies in rats performing odor detection tasks. Physiol. Behav. *41*, 59–69.